EV LIB MODULE CHARACTERIZATION AND ABUSE DETECTION

Nenad Nenadic[1], Matthew Ganter[1], Adam Agosti[1]
[1]Rochester Institute of Technology, 1 Lomb Memorial Dr, Rochester, NY 14623

Primary Topic Area: Innovative Remanufacturing Technologies
Secondary Topic Area: Building a Sustainable Circular Economy for Materials & Products

Abstract

We present the results of an empirical study on accelerated assessment of the remaining capacity of used electric vehicle (EV) lithium-ion battery (LIB) modules in the context of unknown state-of-charge (SOC). The objective was to estimate the state of health (SOH) in the form of the percent capacity fade of individual modules relative to the nominal capacity of a new module. A few percent target accuracy was set to avoid costly full-cycle testing of severely degraded modules. The experimental investigation gave special attention to detecting prior electrical abuse in the form of over-charge and over-discharge. The transient-response waveforms associated with pulse-charge waveforms provided data for fitting the phenomenological equivalent-circuit model (ECM). The model parameters, viz., open-circuit voltage, input impedance, and polarization capacitance, depend on both SOC and SOH, and it was critical to disambiguate the two dependencies. LIB modules of different cathode chemistries required separate characterization of the ECM parameters. Full pulse charge cycles of modules provided data for the capacity fade associated with normal aging. We trained machine-learning models using the estimated parameters of the ECM as features and SOC and SOH as targets. To attain representative model performance, the separation between training and validation data was based on the separation of physical devices: the training dataset employed data associated with a subset of modules, and the validation dataset contained the data from the remaining modules. The initial results on the module from lithium-iron-phosphate (LFP) and nickel manganese cobalt oxides (NMCs) chemistries indicated that the target performance of a few percent accuracy on the capacity fades on the validation data was attained. A separate set of cell-level experiments generated the battery-abuse data by subjecting cells to progressive over-charges and over-discharges. The first results suggest that the increase in the internal impedance exceeds the variance of impedances of the associated moderately degraded modules.

Keywords: EV, LIB repurposing, timed-domain, transient response, SOH estimation, capacity fade, unknown SOC

Introduction and Motivation

The electric vehicle (EV) industry experienced a remarkable acceleration, with lithium-ion battery (LIB) manufacturing rapidly advancing along its technological S-curve. In 2020, global EV production surged to 3.1 million units, representing a substantial 39% increase from the previous year [1]. This impressive growth is just the beginning of a transformative trend in transportation. Market projections paint an even more compelling picture of the EV landscape. Analysts forecast a dramatic expansion, predicting that annual EV production will soar more than eight-fold to 26.9 million vehicles by 2030 [2]. The International Energy Agency (IEA) offers an even more optimistic outlook, anticipating that electric vehicles will constitute 51% of all new vehicle production by 2030 – a sixteen-fold increase that signals a fundamental shift in automotive technology and sustainability when over 1 million EV batteries are expected to reach EOL [3]. Efficient testing of used modules is crucial for successfully processing the anticipated large volumes of retired EV batteries.

Quantitative assessment of battery module performance demands stringent testing methodologies to ensure measurement accuracy and reproducibility. Current industry standards mandate triple-cycle characterization protocols, as single-cycle measurements may yield unreliable results due to environmental variability. Specifically, ambient temperature fluctuations can significantly influence capacity measurements, necessitating multiple cycles to establish statistically robust performance metrics. This approach differentiates between inherent measurement variability and true capacity values, providing a more reliable foundation for subsequent performance analysis.

Lithium-ion batteries with different cathode chemistries require distinct characterization approaches. Nickel manganese cobalt oxides (NMCs), lithium iron phosphates (LFPs), and lithium cobalt oxides (LCOs) exhibit fundamental differences in voltage profiles, internal resistance behavior, and thermal characteristics. These variations necessitate chemistry-specific test protocols to capture the essential parameters for accurate performance modeling. The protocols must account for unique attributes such as the flat voltage profile of LFP cells, the higher voltage sensitivity of NMC chemistries, and the thermal constraints of LCO-based systems.

Safety considerations in battery testing are paramount, particularly regarding the detection of prior abuse or damage. Implementation of robust screening procedures is essential to identify potentially compromised modules before testing, thereby safeguarding both valuable testing equipment and laboratory personnel from potential hazards associated with damaged cells.

In practical applications, particularly when dealing with modules of unknown charge status, there is significant value in developing rapid assessment protocols. A quick diagnostic procedure, approximately ten minutes in duration, would enable efficient triage of modules regardless of their state of charge. This capability would substantially streamline the testing process and improve operational efficiency while maintaining necessary safety standards.

Battery module characterization methods primarily utilize transient response analysis or electrochemical impedance spectroscopy (EIS). This investigation focuses on transient response techniques, which leverage existing cycler infrastructure without requiring specialized impedance measurement equipment. The characterization protocol implements a sequence of galvanostatic pulses interspersed with rest periods of predetermined duration. This pulsed current profile enables the observation of both instantaneous voltage response and relaxation behavior, providing insights into both resistive and capacitive elements of the battery system.

The step-wise current profile serves multiple purposes: it allows for the separation of ohmic resistance from diffusion-related phenomena, enables the quantification of voltage recovery characteristics, and provides data suitable for parameter estimation in equivalent circuit models. The duration of current pulses and rest periods must be optimized to capture relevant time constants while maintaining practical test durations. Typically, rest periods must extend sufficiently to observe voltage relaxation approaching steady state, while current pulses must be long enough to establish quasi-steady-state conditions in the cell.

Review of Related Work

EV batteries reach end of life (EOL) when capacity drops to 70-80% of original, with some failing as early as 90% capacity. Beyond gradual degradation, batteries may be replaced due to "infant mortality" failures from internal cell, module, or component defects [4]. Used batteries offer promising secondary applications in grid storage, performing multiple functions like peak shaving and renewable energy firming [5]. The demand for low-cost storage systems grows with increased deployment of weather-dependent distributed energy resources (DERs) [6]. While firming renewable energy is particularly interesting, stacking different storage capabilities enhances the grid storage system's value proposition [7].

There are many battery models. This work is based on a phenomenological model that fits transient response data (see, e.g., [8]), which was successfully used for a cell-level assessment degradation [9], unlike statistical time-domain health indicators (e.g., kurtosis, RMS, crest factor) as described in [10].

Thermal runaway occurs due to a separator failure induced by electrical, mechanical, or thermal causes [11]. Electrical causes (including prior abuses) were the focus of the study because mechanical abuses are readily visible, and thermal abuse is either a design issue or leads to thermal runaway before the modules are considered for secondary applications. Inducing thermal runaway by thermal and mechanical means are studied elsewhere: for example, Chen et al. [12] studied the effect of SOC in thermal runaway, by triggering the thermal runaway with a uniform heater in a lab environment; Naha et al. [13] induced short mechanically.

Technology Approach

The approach was based on transient response data and the associated ECM model. Data collection included module-level and cell-level testing, where the former provided data for estimating SOH and the latter provided data for abuse detection. The parametrization of the ECM model, introduced in the following subsection, was used for processing both datasets.

Experiments

The study conducted two types of experiments: characterization at a module level and abuse cycles at the cell level. They are described in turn.

Module characterization

The first set of experiments was conducted using a pulse charge and constant current (CC) – constant voltage (CV) discharge at the module level. Figure 1 shows a sample pattern. The pulses served to capture the transient data at different levels of SOC. Coulomb capacities were estimated by integrating total charge during the discharge cycle, which included current taper during the CV stage.

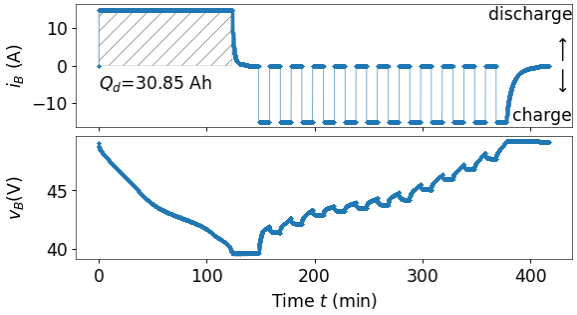

Figure 1 Battery terminal current and voltage in a typical cycle pattern.

The tests were conducted on a commercial cycler using the integrated battery test system Chroma 17020, shown in Figure 2a. We selected a commercial system to make the quick assessment readily deployable. The Chroma system is equipped with a bi-directional power supply, capable of returning the module discharge energy to the grid, which is very valuable feature for reducing the economic and environmental cost associated with testing.

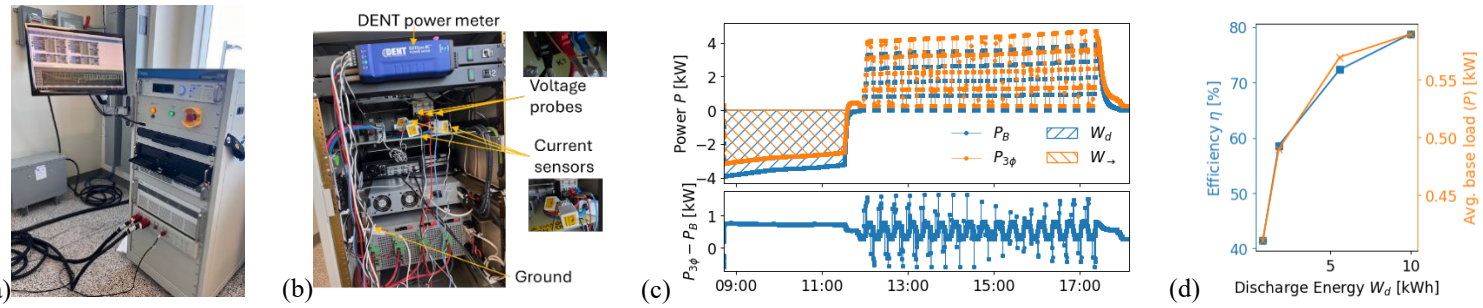

(a) (b) (c) (d)

Figure 2: (a) Chroma 17020 front panel (b) back-panel with power meter (c) example test profile (d) efficiency

The measured efficiency of the system exhibited a dependence on the module size, as shown in Figure 2c. The efficiency of the system increased with the module size. It is plausible that larger commercial systems, with 16 or more channels, have considerably higher efficiency.

Because the characterization is a function of chemistry, the cycles were applied to three different module types, shown in Figure 3b-d, but this paper will focus on the modules shown in Figure 3b because the cells from this module type were subjected to the abuse tests.

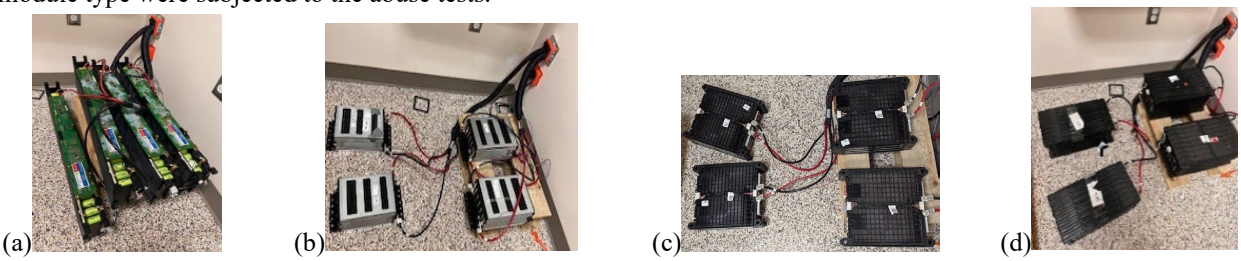

(a) (b) (c) (d)

Figure 3: Modules (a) LFP modules (b)-(d) different versions of NMC modules.

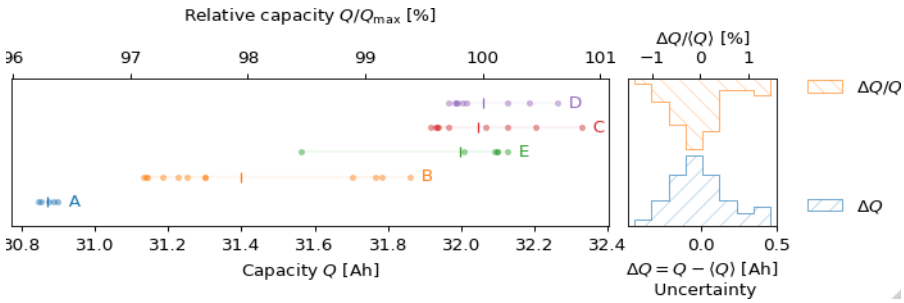

Figure 4 Capacity testing results (NMC modules, shown in Figure 3b).

Figure 4 shows the distribution of repeated capacity measurements for the four modules. The subplot on the left shows individual measurements, with the actual measurements shown on the scale at the bottom, and relative measurement on the top. The differences in capacity were relatively small, but the variation from one test to the next was fairly large.

Cell-abuse testing

Because no existing modules and cells were available at the onset of thermal runaway, RIT experimented with thermal runaway using overcharge. The overcharge experiments induced permanent swelling deformation in cells, as shown in Figure 5. The top row shows the appearance of cell before the first, second, and third overcharge, and the bottom row shows the appearance after these tests. During the third test, the cell outgassed, and some splatters can be seen on the wall to the right of the cell.

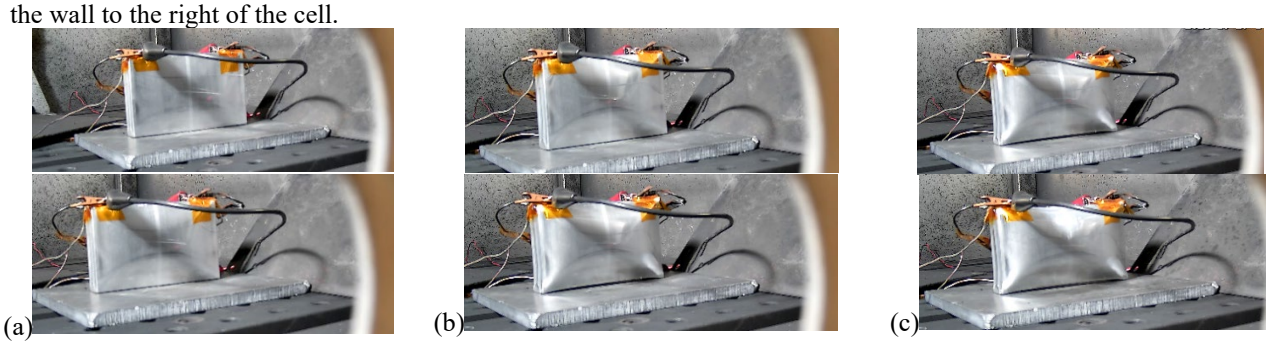

Figure 5 Cell at the start (top) and end (bottom) of overcharge tests (a) cycle 1 (b) cycle 2 (c) cycle 3

Figure 6 shows the waveforms associated with the cyclic overcharging experiment. The characterization was performed at SOC =100%.

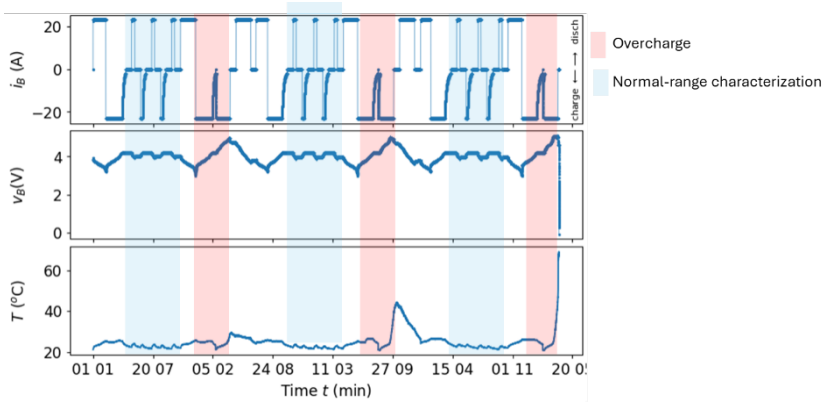

Figure 6: Cyclical characterization and overcharge cycles

Over-discharge experiments were performed by progressively discharging modules beyond their normal voltage level down to zero, with characterization between the deep discharge cycles, as shown in Figure 7. The close up zooms into the last normal range test pattern for characterization. The deep over-discharge cycles (down to zero volts) did not produce observable change in the ECM parameters.

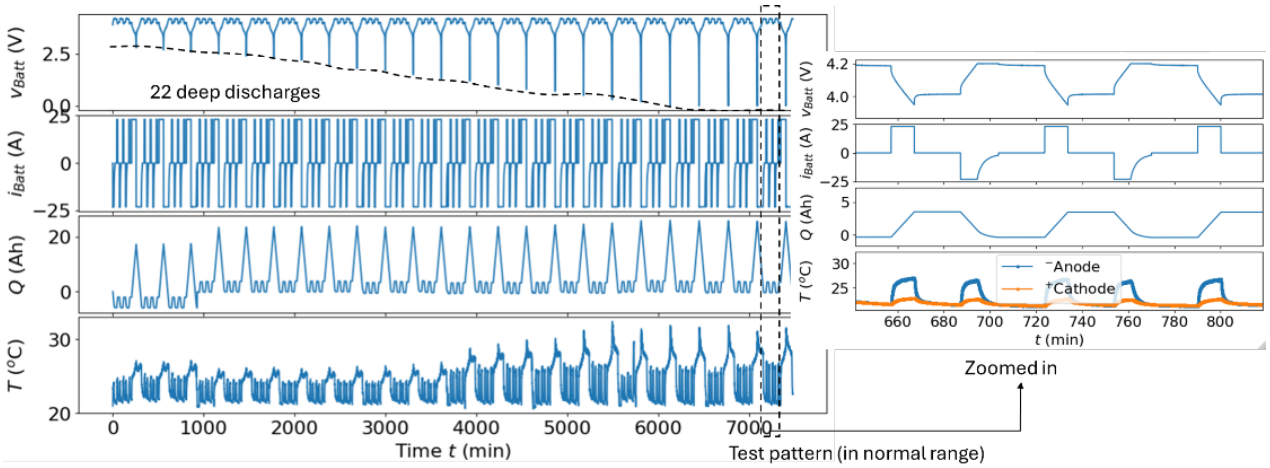

Figure 7 Progressively deeper discharge cycles.

Modeling, Estimation, and Abuse Detection

The ECM model described next, served for processing of experimental data associated with module testing and cell abuse tests. The model parameters were then used to estimate the remaining capacity Q, which we used as the measure of SOH.

Modeling – the ECM Model

This widely-used model (see [8]) can be described as follows: Figure 8a shows the ECM with multiple polarization resistor-capacitor pair, and Figure 8a shows the terminal current i_B and voltage v_B waveforms during a transient response associated with the rest at the end of a pulse-charge. For simplicity, we set the time of the start of the rest period at 0.

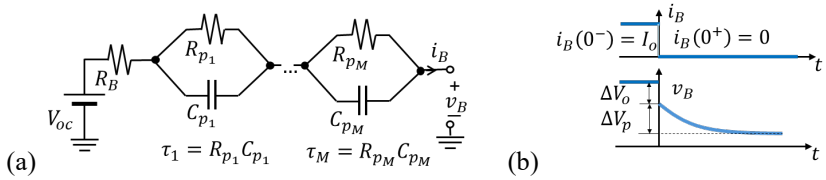

Figure 8 Equivalent circuit model (a) equivalent circuit (b) prototypical v_B and $i_B$at the end of charge pulse

The battery resistance is estimated from the initial step

$$R_B = \frac{\Delta V_o}{i_{B(0^-)}} = \frac{\Delta V_o}{I_o}, \tag{1}$$

where I_o is the current of the pulse ΔV_o denotes the instantaneous voltage change at the beginning of the rest period

$$\Delta V_o = v_B(0^-) - v_B(0^+). \tag{2}$$

The remainder of the transient response serves to estimate the polarization resistor-capacitor pairs $\{(R_{p_m}, C_{p_m})\}_{m=1}^{M}$

$$v_B(t) = V_{oc} - \sum_{m=1}^{M} v_{C_{p_m}}(0)\mathrm{e}^{-\frac{t}{\tau_m}} \quad t > 0. \tag{3}$$

The initial value of the polarization, across all polarization capacitors is denoted by V_p and given by

$$V_p = v_B(0^+) - v_B(\infty) \;=\; I_o \sum_{m=1}^{M} R_{p_m} \tag{4}$$

which yields the initial voltage across a polarization capacitor $C_{p_m}$is

$$v_{C_{p_m}}(0) = \frac{R_{p_m}}{\sum_{m=1}^{M} R_{p_m}} V_p. \tag{5}$$

It is important to emphasize that all circuit parameters in Figure 8a are functions of both SOC and SOH, viz. $V_{oc}(SOC, SOH)$, $R_B(SOC, SOH)$, and $\{(R_{p_m}(SOC, SOH), C_{p_m}(SOC, SOH)\}_{m=1}^{M}$. The model was implemented in Python, and the parameters were estimated the standard open-source library Scipy [14] and its `curve_fit` function.

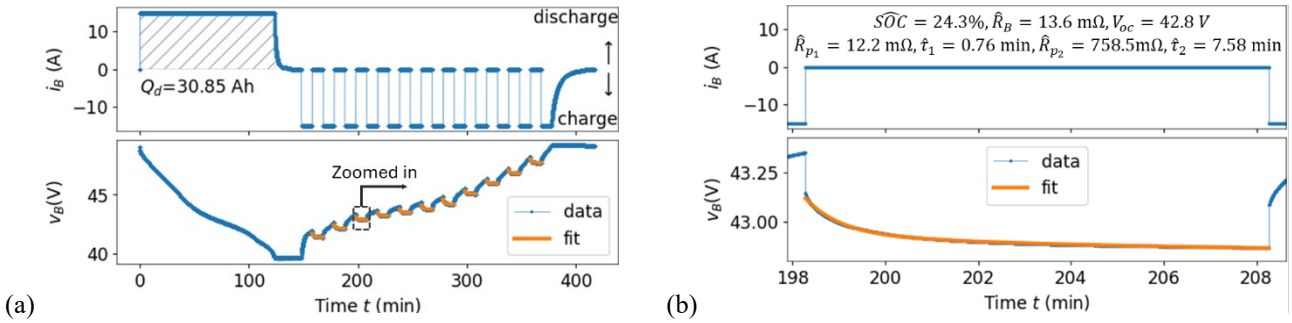

(a) (b)

Figure 9: Module characterization and estimation of model parameters during the rest periods (a) entire test profile (b) close-up showing the fidelity of the fit

Figure 9a shows the fit of the transients for the characterization shown in Figure 1, and Figure 9b zooms into a representative transient, where the number of polarization R-C pairs was 2 (i.e., $M = 2$). The ECM parameters associated with the transient in the close-up, are indicated in the plot. Note that because we used the transient, the current was negative relative to the batteries reference direction.

The symmetry of the two R-C polarization pairs can be problematic for the curve fit, which can randomly assign higher associated time constant ($\hat{\tau}_m = \hat{R}_{p_m}\hat{C}_{p_m}$). To avoid this problem, we always assigned lower-valued fitted time constant to $\hat{\tau}_1$ and higher-valued time constant to $\hat{\tau}_2$, i.e., $\hat{\tau}_1 < \hat{\tau}_2$.

SOH Estimation

A curve fit was applied for multiple characterizations. Figure 10 shows two ($\hat{V}_{oc}$ and $\hat{\tau}_2$) of the six parameters (the polarization R-C parameters were not shown to save space) as a function of SOC and discharge capacity $\hat{Q}$.

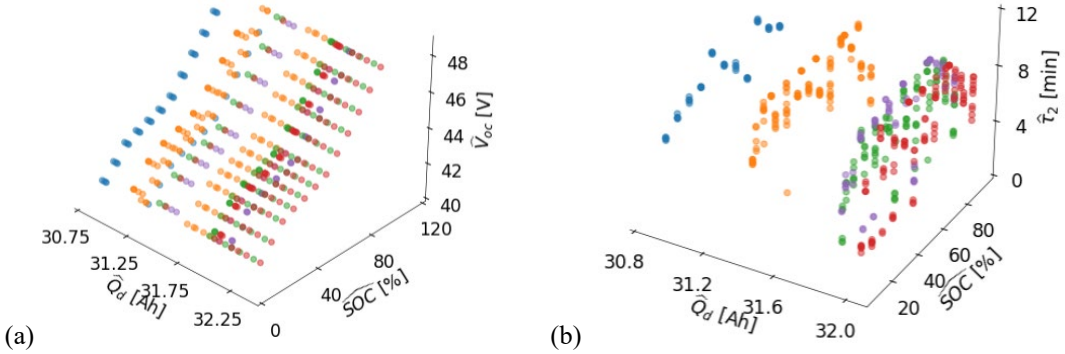

(a) (b)

Figure 10: Estimated parameters (a) Open-circuit voltage $\hat{V}_{oc}$ (b) the larger time constant $\hat{\tau}_2$

The colors denote physical models: for example, all blue dots were estimated on one module, and red on another. The estimation of the discharge capacity $\hat{Q}_d$ was based on the ECM parameters. We collected the parameters in the feature vector, defined as

$$\phi = [\hat{R}_B \;\; \hat{V}_{oc} \;\; \hat{R}_1 \;\; \hat{\tau}_1 \;\; \hat{R}_2 \;\; \hat{\tau}_2] \tag{6}$$

where the estimate time constants $\hat{\tau}_1 = \hat{R}_{p_1}\hat{C}_{p_1}$ and $\hat{\tau}_2 = \hat{R}_{p_2}\hat{C}_{p_2}$ are in minutes, estimated resistances $\hat{R}_B$, $\hat{R}_{p_1}$, and $\hat{R}_{p_2}$ are measured in mΩ, and open-circuit voltage $\hat{V}_{oc}$ is measured in volts. Typical values of the parameters can be seen

Our objective was primarily to estimate $\hat{Q}_d$, but we attempted it in two ways: directly from features, $\hat{Q}_d(\phi)$ or indirectly, by first estimating SOC, $\widehat{SOC} = f(\phi)$ and then , using this to better estimate the discharge capacity $\hat{Q}_d = g(\phi, \widehat{SOC})$. The regression models used in the analyses included Random Forest algorithm, implemented in Scikit-Leand [15] and neural networks implemented in PyTorch [16]. Data associated with two LIB modules was used for training, and the data associated with the remaining two LIB modules was used for validation. Allocating all data from a specific physical object exclusively to either training or validation datasets offers a significant advantage: the validation results will more accurately predict real-world performance, as the deployed system will encounter entirely different physical objects (LIB modules, in our case). Additionally, immediate neighbors, such as consecutive cycles, often exhibit high similarity, which can create excessive overlap between training and validation data. While using consecutive cycles across both sets might temporarily show improved performance with reduced validation error, this

approach creates an artificially optimistic assessment that fails to represent realistic deployment conditions. The training and validation errors associated by both a direct regression model $\hat{Q}_d(\phi)$ and its indirect counterpart $\hat{Q}_d = g(\phi, \widehat{SOC})$, both implemented in the form of Random Forest algorithm, are shown in Figure 11. Both training and validation error are within $\pm 2\%$ for both SOC and discharge capacity estimates. Neural network models produced similar results.

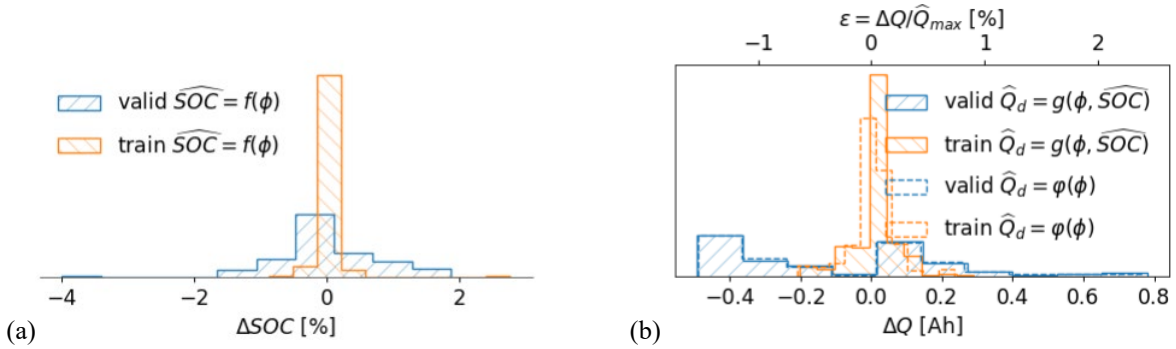

Figure 11: Distribution of regression model errors (a) SOC estimation (b) discharge capacity estimation

In addition, to regression using the ECM parameters, we estimated parameters directly from the waveforms, and obtained similar, slightly better results, as shown in Figure 12.

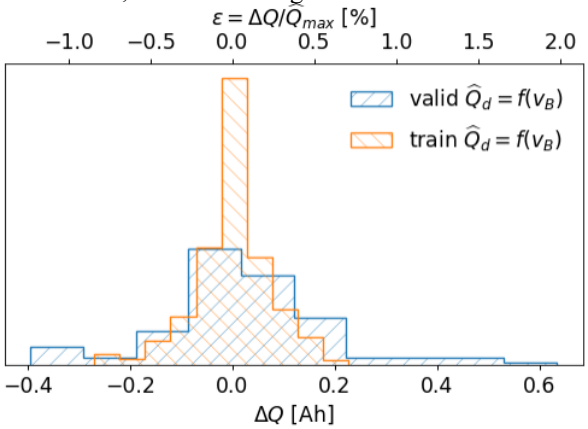

Figure 12 Training and validation error of the estimated remaining capacity using raw transient data.

Abuse detection

We used a similar approach for the abuse detection. The ECM model parameters were estimated from transient data associated with test pattern between the overcharge periods (see blue shaded sections in Figure 6). Figure 13 shows the estimated ECM parameters and the cell temperature. Three cycles were completed before the cell failed were labeled *pre-abuse*, *after 1st abuse*, and *after 2nd abuse*. Of the six parameters, $\hat{R}_B$ the most compelling, monotonical dependence on the abuse.

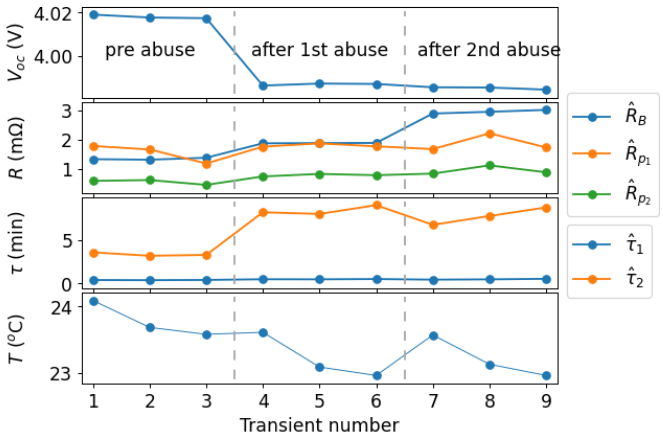

Figure 13: Estimated ECM parameters from overcharge abuse data.

Figure 14a shows the histograms of 495 estimates of battery resistance $\hat{R}_B$ of modules (see also Figure 10b). The bottom x-axis provides the scale for module-level $\hat{R}_B$ and the top x-axis average cell-level $\hat{R}_{B_{cell}} = \hat{R}_{B_{module}}/12$ because module was comprised of twelve cells connected in series.

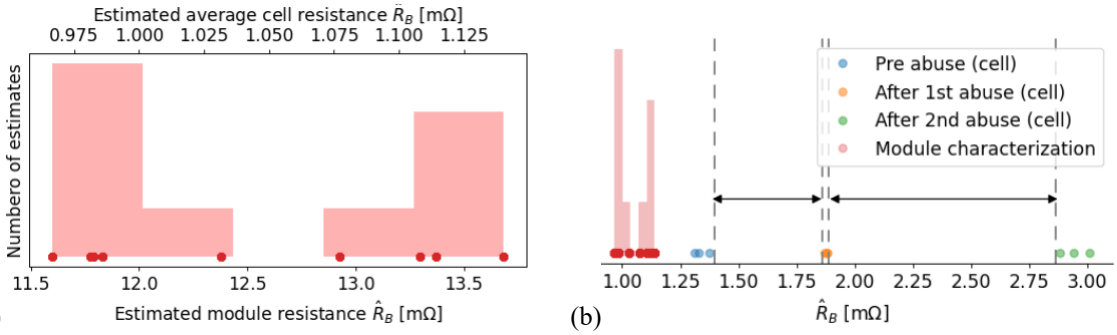

Figure 14: (a) Module-level estimations with average cell scale (b) cell-abuse and module level estimates

Figure 14b combines the $\hat{R}_B$ cell estimates from Figure 13 with $\hat{R}_B$ estimates from module experiments scaled to cells. Before abuse (blue dots) cells, had slightly higher values than those computed from new modules (red dots). The estimates after the first abuse (orange dots) was distinctly higher than pre-abuse, and the points after the second abuse (green dots) had even higher margin relative to the estimates after the first abuse. The clear margins, signified by arrows, showed that the abused cells were detectable from the normal cells and modules.

Discussion

This paper shows module characterization of one of the four module types that have been investigated. Unfortunately, the variation of degradation among modules was negligible because the modules had not seen significant variation. Therefore, full characterization tests were repeated many times to induce variation during cycling. The four battery types, shown in Figure 3, had respectively, 71, 51, 48, and 220 tests cycles, of the form shown in Figure 1. Generally, characterizations of LIBs, upon which EIS and transient methods rest, are expensive and time consuming. Battery model parameters are chemistry-dependent, with small cathode chemistry variations significantly affecting parameters. This necessitates repeated characterization for each chemistry variant.

The solid-state fuel gauge industry exemplifies this challenge. LIB in consumer electronics like laptops and cell phones require full characterization to configure fuel solid-state fuel gauge parameters. Even small, incremental modifications of cathode chemistry changes, require new characterization. The complexity stems from model parameters' dependence on both SOC and SOH ($\hat{Q}_d$), which must be established empirically.

We found that, in addition to SOC and $\hat{Q}_d$, the ECM parameters depend on the current level. Figure 15a shows a cell-level characterization test at four different pulse current levels $I_p \in \{2, 5, 10, 15\}$ A, and Figure 15b shows the battery estimates associated with transients at the end of pulse charges (EOC) and the end of pulse discharges (EOD). The variations of the estimates were significant, despite relatively small variation in SOC (because the charge and discharge pulse alternated).

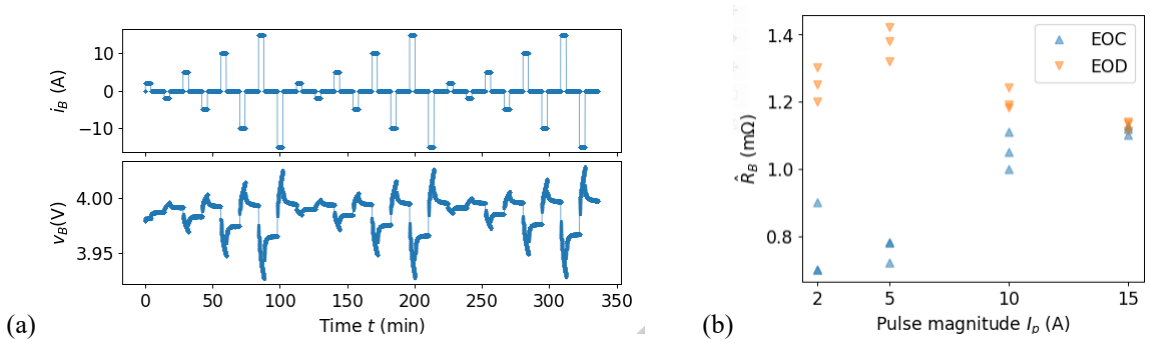

Figure 15 Current level test (a) waveforms (b) resistance estimates

We explored the remaining discharge capacity and SOC from the voltage waveform data, using machine learning models, and achieved similar and sometimes slightly better results compared to the models that operated on the estimated ECM parameters. However, models based on the ECM parameters had a significant advantage: the ECM values offered better interpretability of the results than a black-box approach that operates directly on the raw data. For example, reduced capacity can be related to increased battery resistance or reduced time constants.

Conclusion & Recommendations.

We presented the results of an empirical study for estimating remaining capacity of used LIB modules and cells recovered from EV batteries. The first objective was to estimate capacity within a few percent to avoid costly cycle tests on severely degraded modules. The estimated remaining discharge capacity was within ±2%, which is probably sufficient.

The second objective was to detect modules which suffered prior abuse. Because mechanical abuse is visible, the focus of the study was on electrical abuse in the form of overcharge and over-discharge. The abuse tests were conducted at the cell to limit the power of potential explosion. The results of over-charge experiments showed promise, as the battery-resistance estimates associated with abuses had progressive large margins relative to pre-abuse tests. The deep discharge tests did not show evidence of change, when measured by the model parameters.

Future work will include cell-level deep discharge abuse tests with longer, up to two days, rest periods at the end of deep discharge and will include full characterization, at multiple levels of SOC (not just SOC=100%) between overcharge cycles.

Acknowledgments

This material is based upon work supported by the U.S. Department of Energy's Office of Energy Efficiency and Renewable Energy (EERE) under the Advanced Manufacturing Office Award Number DE-EE0007897 awarded to the REMADE Institute, a division of Sustainable Manufacturing Innovation Alliance Corp. In addition, RIT received funding, in part, from New York State Empire State Development under Grant #AC118 that supported the work on this project.

The views expressed herein do not necessarily represent the views of the U.S. Department of Energy or the United States Government or New York State.

References

[1] Jones, C., 2021, "Global Electric Vehicle Sales up 39 % in 2020 as Overall Car Market Collapses," (February), pp. 2020–2022 [Online]. Available: https://www.businesswire.com/news/home/20210208005423/en/Canalys-Global-Electric-Vehicle-Sales-up-39-in-2020-as-Overall-Car-Market-Collapses. [Accessed: 12-Jul-2021].

[2] "Electric Vehicle Market Share, Forecast | Growth Analysis & Opportunities [2030]" [Online]. Available: https://www.marketsandmarkets.com/Market-Reports/electric-vehicle-market-209371461.html. [Accessed: 29-Jan-2024].

[3] Kelleher Environmental, 2019, "Research Study on Reuse and Recycling of Batteries Employed in Electric Vehicles: The Technical, Environmental, Economic, Energy and Cost Implications of Reusing and Recycling EV Batteries," p. 206.

[4] Nenadic, N. G., Trabold, T. A., and Thurston, M. G., 2020, "Cell Replacement Strategies for Lithium Ion Battery Packs," Batteries, **6**(3), p. 39.

[5] Valant, C., Gaustad, G., and Nenadic, N., 2019, "Characterizing Large-Scale, Electric-Vehicle Lithium Ion

Transportation Batteries for Secondary Uses in Grid Applications," Batteries, **5**(1).
[6] Piggott, C. E., Caruso, Z., and Nenadic, N. G., 2023, "Low-Cost Communication Interface between a Smart Meter and a Smart Inverter," Energies, **16**(5).
[7] Byrne, R. H., Hamilton, S., Borneo, D. R., Olinsky-Paul, T., and Gyuk, I., 2017, "The Value Proposition for Energy Storage at the Sterling Municipal Light Department," *2017 IEEE Power & Energy Society General Meeting*, pp. 1–5.
[8] Min, C., and Rincon-Mora, G. A., 2006, "Accurate Electrical Battery Model Capable of Predicting Runtime and I-V Performance," Energy Conversion, IEEE Trans., **21**(2), pp. 504–511.
[9] Nenadic, N. G., Bussey, H. E., Ardis, P. A., and Thurston, M. G., 2014, "Estimation of State-of-Charge and Capacity of Used Lithium-Ion Cells," Int. J. Progn. Heal. Manag., **5**(2).
[10] El-Dalahmeh, M., Thummarapally, P., Al-Greer, M., and El-Dalahmeh, M., 2021, "Time and Frequency Domain Health Indicators for Capacity Prediction of Lithium-Ion Battery," 2021 56th Int. Univ. Power Eng. Conf. Powering Net Zero Emiss. UPEC 2021 - Proc.
[11] Liao, Z., Zhang, S., Li, K., Zhang, G., and Habetler, T. G., 2019, "A Survey of Methods for Monitoring and Detecting Thermal Runaway of Lithium-Ion Batteries," J. Power Sources, **436**, p. 226879.
[12] Chen, H., Buston, J. E. H., Gill, J., Howard, D., Williams, R. C. E., Rao Vendra, C. M., Shelke, A., and Wen, J. X., 2020, "An Experimental Study on Thermal Runaway Characteristics of Lithium-Ion Batteries with High Specific Energy and Prediction of Heat Release Rate," J. Power Sources, **472**, p. 228585.
[13] Naha, A., Khandelwal, A., Agarwal, S., Tagade, P., Hariharan, K. S., Kaushik, A., Yadu, A., Kolake, S. M., Han, S., and Oh, B., 2020, "Internal Short Circuit Detection in Li-Ion Batteries Using Supervised Machine Learning," Sci. Reports 2020 101, **10**(1), pp. 1–10.
[14] Jones, E., Oliphant, T., and Peterson, P., 2001, "SciPy: Open Source Scientific Tools for Python," http//www. scipy. org/.
[15] Pedregosa, F., Varoquaux, G., Gramfort, A., Michel, V., Thirion, B., Grisel, O., Blondel, M., Prettenhofer, P., Weiss, R., and Dubourg, V., 2011, "Scikit-Learn: Machine Learning in Python," J. Mach. Learn. Res., **12**, pp. 2825–2830.
[16] Paszke, A., Gross, S., Massa, F., Lerer, A., Bradbury Google, J., Chanan, G., Killeen, T., Lin, Z., Gimelshein, N., Antiga, L., Desmaison, A., Xamla, A. K., Yang, E., Devito, Z., Raison Nabla, M., Tejani, A., Chilamkurthy, S., Ai, Q., Steiner, B., Facebook, L. F., Facebook, J. B., and Chintala, S., 2019, "PyTorch: An Imperative Style, High-Performance Deep Learning Library," Adv. Neural Inf. Process. Syst., **32**.

About the Authors

Nenad Nenadic is a Research Associate Professor at RIT. He received a Ph.D in Electrical and Computer Engineering from the University of Rochester in 2001. His research interests include sensors, battery systems, automation, and machine learning.
Matthew Ganter is the Director of the Battery Development Center (BDC) and Assistant Research Professor of Chemical Engineering at Rochester Institute of Technology (RIT). The RIT BDC is a state-of-the-art research and rapid prototyping and testing facility focused on the development and qualification of emerging energy storage technologies. Dr. Ganter's research focuses on nanomaterials, energy storage, and sustainable energy technologies, particularly emphasizing high-energy density lithium-ion designs. Dr. Ganter holds a Ph.D. in Sustainability from RIT and has authored or co-authored 22 peer-reviewed publications, with over 1800 citations to his name.
Adam Agosti is a Senior Engineer at RIT. He received his Bachelor of Science in Mechanical Engineering from the University at Buffalo in 2006. He has primarily worked in the automotive industry doing algorithm development before transitioning to RIT.